Synthesis and Photoluminescence Properties of Eu3+-Doped Na2YMg2V3O12: A Novel Red-Emitting Phosphor for White-Light-Emitting Diodes

Weiyi Zhang
Qilu University of Technology
Yanqiu Shao
Qilu University of Technology
Ying Zhu (zhuyingee@163.com)
Qilu University of Technology
Yingying Shao
Qilu University of Technology
Zhaohui Huang
China University of Geosciences Beijing
Min Xin
China University of Geosciences Beijing
Yangai Liu
China University of Geosciences Beijing
Can He
China University of Geosciences Beijing
Xiaoguang Zhang
Beijing University of Technology

Research Article

Keywords: Na2YMg2V3O12, Eu3+, red emission, energy transfer, luminescence, WLEDs

Posted Date: July 27th, 2021

DOI: https://doi.org/10.21203/rs.3.rs-736843/v1

Synthesis and photoluminescence properties of Eu^{3+}-doped $Na_2YMg_2V_3O_{12}$: A novel red-emitting phosphor for white-light-emitting diodes

Weiyi Zhang[a, 1], Yanqiu Shao[a, 1], Ying Zhu[a, *], Yingying Shao[a], Zhaohui Huang[b], Min Xin[b], Yangai Liu [b], Can He[b, **], Xiaoguang Zhang[c]

[a]Advanced Materials Institute, Qilu University of Technology (Shandong Academy of Sciences),Jinan 250014, China

[b]Beijing Key Laboratory of Materials Utilization of Nonmetallic Minerals and Solid Wastes, National Laboratory of Mineral Materials, School of Materials Science and Technology, China University of Geosciences, Beijing 100083, China

[c]Institute of Circular Economy, Beijing University of Technology, Beijing, China

[1] Weiyi Zhang and Yanqiu Shao contributed equally to this work.

[*, **] Corresponding authors.

E-mail: Ying Zhu, zhuyingee@163.com

Can He, hecan1221@163.com

Abstract

The fabrication and luminescent properties of novel $Na_2YMg_2V_3O_{12}:Eu^{3+}$ phosphors produced by conventional solid-state reactions were investigated. Self-activated emission of the $Na_2YMg_2V_3O_{12}$ host produces a broad emission band ranging from 400 to 700 nm with a maximum peak at 530 nm, ascribed to the charge transfer in the $(VO_4)^{3-}$ groups. Excitation with near-UV (365 nm) light causes the $Na_2YMg_2V_3O_{12}:Eu^{3+}$ phosphors to emit bright red light, including both the broad emission band of the $(VO_4)^{3-}$ groups and the sharp emission peaks of Eu^{3+} ions. At a quenching concentration of 0.03 mol, the Eu^{3+} ion emission peaks were located at 597, 613, 654 and 710 nm. As-prepared $Na_2YMg_2V_3O_{12}:Eu^{3+}$ phosphors also exhibited stable emission at high temperatures. Furthermore, a designed and packaged white-light-emitting diode (WLED) lamp, including the obtained phosphors, commercial $(Ba,Sr)_2SiO_4:Eu^{2+}$ green phosphors, $BaMgAl_{10}O_{17}:Eu^{2+}$ blue phosphors and a near-ultraviolet (n-UV) chip, emitted bright white light with a good chromaticity coordinate of (0.3068, 0.3491), a satisfactory colour rendering index of 88.20 and a properly correlated colour temperature of 4460.52 K. These results indicate the potential of this $Na_2YMg_2V_3O_{12}:Eu^{3+}$ phosphor as a red-emitting phosphor for solid-state illumination.

Keywords: $Na_2YMg_2V_3O_{12}$; Eu^{3+}; red emission; energy transfer; luminescence; WLEDs

1. Introduction

White-light-emitting diodes (WLEDs) are widely used as light sources in instruments, traffic lights and large-area display screens because of their low heat generation, low power consumption, high durability, fast response speed and small size[1-3]. Most WLED devices implement InGaN-based blue LED chips with the yellow phosphor $YAG:Ce^{3+}$ due to the lack of a reliable red light component. This implementation has limitations of low (<75) colour rendering index (Ra) and high colour temperature (>4500 K)[4-8]. Two common methods provide solutions to the

above problems: One method combines the blue LED chips (420–470 nm) with red and green phosphors, and another promising method is based on red, green and blue phosphors stimulated by near-ultraviolet (n-UV) LED chips (350–410 nm). Both of these methods require high-efficiency red phosphors[9-12].

It is known that a broad emission peak or multiple emission peaks in the visible region provide white light with an appropriate CRI and accurate colour rendering[13-16]. Vanadate, composed of VO_4^{3-} tetrahedral, constitutes an important phosphor host that shows a broadband emission band at 400–700 nm, high luminous efficiency and excellent chemical stability upon excitation by n-UV light.[17, 18] Vanadate phosphors produce intense visible emissions corresponding to the $V^{5+}\rightarrow O^{2-}$ charge transfer (CT) transition in the VO_4^{3-} tetrahedron[19]. In addition, rare earth ion-activated vanadate phosphors can give rise to visible emissions that can be tuned by the energy transfer between VO_4^{3-} and rare earth ions[20, 21]. The Eu^{3+} ion is a classical activator for efficient red phosphors and has been widely investigated because of its characteristic red emissions arising from $^5D_0\rightarrow{}^7F_J$ (J = 0, 1, 2, 3, 4) transitions. Among these transitions, the dominant 610–630 nm emission from the $^5D_0\rightarrow{}^7F_2$ electric dipole transition is conducive to the improvement of the colour purity of the phosphor, in which Eu^{3+} occupies the lattice sites lacking centro-symmetry[22]. Among such phosphors, tetragonal zircon-type $LnVO_4$ (Ln = Y, La, Gd) has been widely studied as a luminescent matrix, and $YVO_4:Eu^{3+}$ red phosphor has been used in high-pressure mercury lamps, plasma flat-panel displays and other applications[23, 24]. Novel single-garnet-structure $Na_2LnMg_2V_3O_{12}$ (Ln = Y, Gd) was first synthesised by Guo[25], but few studies report the luminescent properties of these rare earth ion-doped compounds. Recently, researchers have investigated materials such as $Ba_2BiV_3O_{11}:Eu^{3+}$[26], $Ca_2NaMg_2V_3O_{12}:Eu^{3+}$[27] and $Na_3Gd(VO_4)_2:Eu^{3+}$[28]. The discovery of a new, efficient, self-activated, luminescent, Eu^{3+}-doped vanadate material would be highly desirable.

In this work, a series of red-emitting $Na_2YMg_2V_3O_{12}:Eu^{3+}$ phosphors were prepared via high-temperature solid-state reactions. The phase purities, morphologies, decay times and photoluminescence properties of the as-prepared $Na_2YMg_2V_3O_{12}:Eu^{3+}$ phosphors were studied in detail. A WLED lamp was designed and packaged, further confirming the feasibility of these red-emitting phosphors for implementation in conventional indoor lighting.

2. Experimental process

Each $Na_2YMg_2V_3O_{12}$ host lattice phosphor, $Na_2YMg_2V_3O_{12}:xEu^{3+}$ (x = 0.01, 0.04, 0.08, 0.12, 0.16, 0.20, 0.24), was prepared via a high-temperature solid-state reaction. The analytical reagents $NaHCO_3$, $Mg(OH)_2$ and NH_4VO_3 and the high-purity rare earth oxides Y_2O_3 (99.99%) and Eu_2O_3 (99.99%) were used as raw materials. It is noteworthy that 5 mol% excesses of $NaHCO_3$ and $Mg(OH)_2$ were needed to compensate for volatilisation losses. All of these chemicals were mixed homogeneously in an agate mortar for approximately 30 min and pre-heated in a muffle furnace at 500 °C for 6 h, followed by heating at 800 °C for 6 h in air. After cooling to room temperature naturally, each sample was ground into powder for measurement.

The LED devices were fabricated with the as-prepared $Na_2YMg_2V_3O_{12}:xEu^{3+}$ phosphors,

commercial $(Ba, Sr)_2SiO_4$: Eu^{2+} green phosphors, $BaMgAl_{10}O_{17}:Eu^{2+}$ blue phosphors, and an InGaN chip with a dominant emission at 365 nm (Shenzhen Looking Long Technology Co., Shenzhen, China). First, the phosphors were thoroughly mixed with organic silica gel. The weight ratio of total phosphors to organic silica gel is about 1:5. The silica gel used to package LED chips needs excellent light transmittance[29], and the light transmittance of the silica gel we chose is 96% (thickness of 1mm). Then, the surfaces of the InGaN chips were coated with the mixture with an approximate thickness of 0.5 mm. Finally, the chips were dried at 135 °C for 2h and the LED devices was obtained.

The powder X-ray diffractometer (XRD-6000, SHIMADZU, Kyoto, Japan) with Cu Kα radiation (λ = 0.15406 nm) was used to measure the phase composition of the as-prepared samples with a 40 kV operating voltage and 30 mA current. The microscopic morphology of the as-synthesized sample was investigated by a field-emission scanning electron microscope (SEM, Model Zeiss Supra-55, Heidenheim, Germany). The fluorescence spectrophotometer (F-4600, HITACHI, Tokyo, Japan) equipped with a 150 W Xe lamp as an excitation source was utilized to measure the photoluminescence (PL) and photoluminescence excitation (PLE) spectra at room temperature under 400 V of operating voltage (Xe lamp). The photoluminescence spectrum of the selected phosphor, which is temperature-dependent, was examined using a computer-controlled electric furnace spectrophotometer (TAP02, Orient KOJI, Tianjin, China). The phosphor powder was heated with a heating rate of 50 °C/min, and held at each test temperature for 3 min. The PL decay curves were obtained through a spectrofluorometer (TBX-PS, HORIBA Jobin Yvon, Paris, France). Quantum yield (QY), defined as the ratio of the emitted photons to the absorbed photons, was measured by a spectrofluorometer (FLS1000, EDINBURGH, Livingston, Britain) equipped with an integrating sphere. The electroluminescence spectra, CCT, and Ra of the packed LED devices were measured using a UV-vis-near IR spectrophotocolorimeter (PMS-80, Everfine, Hangzhou, China).

3. Results and discussion

3.1. Phase and crystal structure of $Na_2YMg_2V_3O_{12}:Eu^{3+}$

The phase compositions and crystal structures of the as-prepared powder samples were characterised at room temperature. The XRD patterns of $Na_2YMg_2V_3O_{12}:xEu^{3+}$ (x = 0.01, 0.04, 0.08, 0.12, 0.16, 0.20, 0.24) samples collectively exhibited main peaks at 17.5°, 20.3°, 28.8°, 32.3°, 33.9°, 35.5°, 36.9°, 51.0°, 53.2° and 55.4° (Fig. 1a), corresponding, respectively, to the (2 1 1), (2 2 0), (4 0 0), (4 2 0), (3 3 2), (4 2 2), (4 3 1), (4 4 4), (6 4 0) and (6 4 2) planes of a single garnet structure with cubic space group Ia3d (No. 230). All of these diffraction peaks of the $Na_2YMg_2V_3O_{12}:xEu^{3+}$ samples match well with the standard profile of $Na_2YMg_2V_3O_{12}$ (PDF No. 49-0412). These results indicate that the Eu^{3+} ion doping does not significantly affect the crystalline structure of $Na_2YMg_2V_3O_{12}$. In general, a new solid solution can be formed when the percentage difference in radii between substituted ions and dopant ions is less than 30%. The percentage difference in radii between Y^{3+} (substituted ion) and Eu^{3+} (dopant ion) can be estimated using the expression[11]

$$D_r = \frac{R_m(CN) - R_d(CN)}{R_m(CN)} \times 100\%, \quad (1)$$

where D_r is the percentage difference in radii, and $R_m(CN)$ and $R_d(CN)$ are the ionic radii of the substituted ion and dopant ion, respectively. Here, the radii of Y^{3+} and Eu^{3+} ions are 0.90 and 0.95 Å, respectively. As a result, the D_r value was calculated to be approximately 5.56%, which is less than 30%. This calculation further revealed that Eu^{3+} ions can easily replace Y^{3+} ions to be incorporated into $Na_2YMg_2V_3O_{12}$ host lattices.

A spatial structural schematic of the garnet-structured $Na_2YMg_2V_3O_{12}$ unit cell is pictured in Fig. 1(b). As implied, the alkali metal Na^+ ions and rare earth Y^{3+} ions occupy the A sites, coordinating with eight O^{2-} ions to form a dodecahedron with D2 symmetry (lacking an inversion centre). Meanwhile, the alkaline earth metal Mg^{2+} ions are located in octahedral B sites bonded with six oxygen atoms, and the V^{5+} ions (in VO_4^{3-}) are located in Td sites surrounded by four O^{2-} ions. Owing to the similar cation radii and the equal valence of Y^{3+} and Eu^{3+}, the Y^{3+} ion position can be easily occupied by Eu^{3+} ions in the host lattice without any structural transformation. The same XRD patterns for $Na_2YMg_2V_3O_{12}$:Eu^{3+} and the $Na_2YMg_2V_3O_{12}$ standard further confirm that the Eu^{3+} ions are doped in the $Na_2YMg_2V_3O_{12}$ host at the Y^{3+} sites.

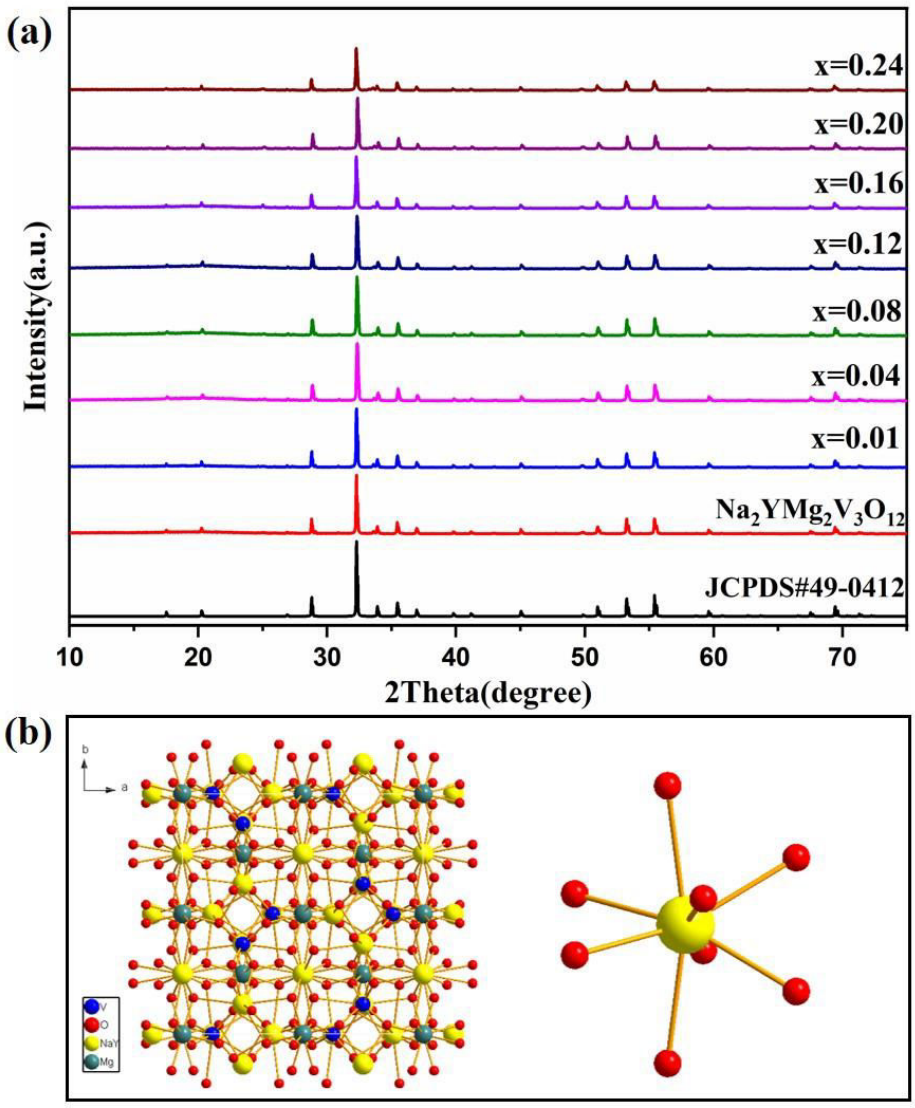

Fig. 1. (a) XRD patterns of $Na_2YMg_2V_3O_{12}$:xEu^{3+} (x=0, 0.01, 0.04, 0.08, 0.12, 0.16, 0.20, 0.24) phosphors and the standard pattern of $Na_2YMg_2V_3O_{12}$ (JCPDS 49–0412), (b) the schematic crystal structure of $Na_2YMg_2V_3O_{12}$ compound

3.2. Luminescence properties of $Na_2YMg_2V_3O_{12}$:Eu^{3+} phosphors

The PLE and PL spectra of an undoped $Na_2YMg_2V_3O_{12}$ sample are presented in Fig. 2(a). The $Na_2YMg_2V_3O_{12}$ sample shows a broad absorption band from 250 to 400 nm, which could match the near-UV LED chip for use in WLEDs. Under excitation at 365 nm, the as-prepared $Na_2YMg_2V_3O_{12}$ sample also emitted a broad emission ranging from 400 to 700 nm, with a maximum at 530 nm. This emission is attributed to the CT of an electron from the oxygen 2p orbital to the vacant 3d orbital of V^{5+} in tetrahedral $(VO_4)^{3-}$ groups[30]. The emission band whose maximum lies at 530 nm can be further decomposed by Gaussian peak separation into two sub-bands centred at 324 and 366 nm respectively. As shown in Fig. 2(b), the $(VO_4)^{3-}$ group has a ground-state $^1A_1$ and excited states $^1T_1$, $^1T_2$, $^3T_1$ and $^3T_2$. The decomposed emission sub-bands are attributed to the $^3T_2 \rightarrow {}^1A_1$ (Em_1 = 512 nm) and $^3T_1 \rightarrow {}^1A_1$ (Em_2 = 571 nm) transitions of the $(VO_4)^{3-}$ groups. Moreover, the excitation band is composed of two sub-bands, which can be

assigned to the $^1A_1 \rightarrow {}^1T_2$ (Ex_1 = 324 nm) and $^1A_1 \rightarrow {}^1T_1$ (Ex_2 = 366 nm) transitions of the $(VO_4)^{3-}$ groups.

Fig. 2(b) shows the PLE and PL spectra of the $Na_2YMg_2V_3O_{12}$:0.2Eu^{3+} phosphor at room temperature. As shown in Fig. 2(b), the excitation spectrum for $Na_2YMg_2V_3O_{12}$:0.2Eu^{3+} monitored at 613 nm shows a broad band similar to that of samples lacking dopant ion Eu^{3+}. This similarity may result from the energy transfer behaviour from $(VO_4)^{3-}$ to Eu^{3+} and the complete overlap between the excitation spectra of $(VO_4)^{3-}$ and Eu^{3+}. The broad excitation spectrum of the $Na_2YMg_2V_3O_{12}$:Eu^{3+} sample indicates that it can be efficiently excited by n-UV light, making it well matched with n-UV LED chips. Also observed are the broad emission band at 530 nm due to the CT transitions of the $(VO_4)^{3-}$ groups, as well as emission peaks at 597 nm ($^5D_0 \rightarrow {}^7F_1$), 613 nm ($^5D_0 \rightarrow {}^7F_2$), 654 nm ($^5D_0 \rightarrow {}^7F_3$) and 710 nm ($^5D_0 \rightarrow {}^7F_4$) due to Eu^{3+} ions. According to Judd–Ofelt theory, the number and relative intensity of $^5D_0 \rightarrow {}^7F_J$ transitions can vary with the variation in the crystal field environment of Eu^{3+} ions[31]. $^5D_0 \rightarrow {}^7F_2$ emission is dominated by the electric dipole transition, which occurs only when Eu^{3+} ions occupy the lattice sites lacking inversion symmetry[32]. On the contrary, when Eu^{3+} ions occupy the lattice sites with inversion symmetry, the $^5D_0 \rightarrow {}^7F_1$ magnetic transition dominates. In the $Na_2YMg_2V_3O_{12}$:Eu^{3+} sample, the $^5D_0 \rightarrow {}^7F_2$ electric dipole transition located at 613 nm is much stronger than the $^5D_0 \rightarrow {}^7F_1$ magnetic dipole transition located at 597 nm, thus confirming that Eu^{3+} ions are located at the non-centro-symmetric sites in the point group.

PL spectra for $Na_2YMg_2V_3O_{12}$:xEu^{3+} (x = 0.01, 0.04, 0.08, 0.12, 0.16, 0.20, 0.24) samples with different doping concentrations are shown in Fig. 2(c). As the Eu^{3+} concentration increases, the position and shape of the emission peak remain almost unchanged. Emission intensity increases initially with increasing Eu^{3+} concentration, reaches a maximum at an Eu^{3+} concentration of x = 0.20 and then decreases with further concentration increase due to the concentration quenching effect. The host emission of the $(VO_4)^{3-}$ groups has an intensity comparable with that of the Eu^{3+} emission in the 1% doped sample. At a doping concentration of 20%, the intensity of the host emission is much lower, and Eu^{3+} emission dominates the emission spectrum. Fig. 2(d) shows the concentration dependence of $(VO_4)^{3-}$ and Eu^{3+} emission intensity. With increasing Eu^{3+} concentration, the emission intensity of $^5D_0 \rightarrow {}^7F_2$ grows drastically and the emission intensity of the $(VO_4)^{3-}$ groups decreases. This finding also indicates energy transfer from the $(VO_4)^{3-}$ groups to Eu^{3+}.

Fig. 3 shows a schematic diagram of the energy transfer between $(VO_4)^{3-}$ and Eu^{3+}. In the matrix undoped with Eu^{3+}, $(VO_4)^{3-}$ ground-state absorption energy occurs in the $^1A_1 \rightarrow {}^1T_1$ and $^1A_1 \rightarrow {}^1T_2$ transitions and decays to $^3T_1$ and $^3T_2$ non-radiatively. When the matrix is doped with Eu^{3+} at an excitation wavelength of 365 nm, part of the energy of $^3T_1$ and $^3T_2$ is transferred to the $^5D_0$ excited state of Eu^{3+}; the radiative transition then leads to red light emission. Therefore, in the emission spectrum of $Na_2YMg_2V_3O_{12}$:Eu^{3+}, both the charge transition band of $(VO_4)^{3-}$ and the characteristic f–f transition emission peak of Eu^{3+} can be observed.

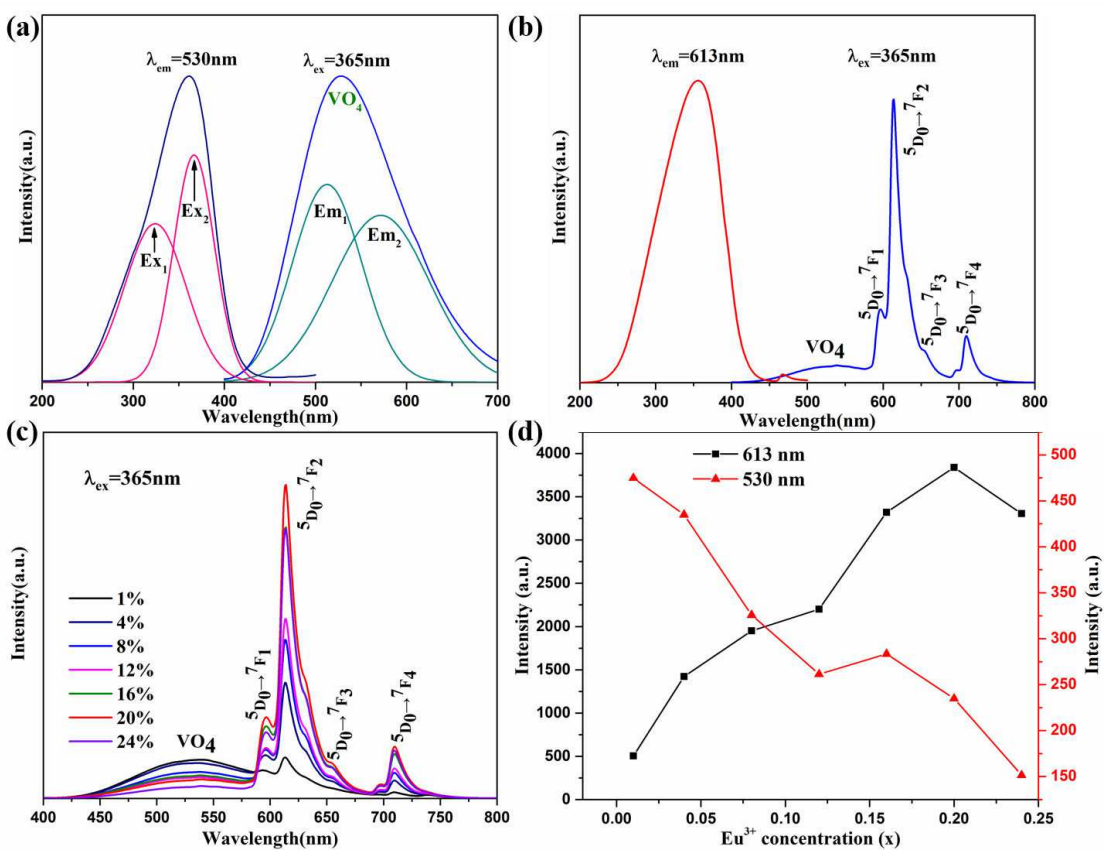

Fig. 2. (a) PLE and PL spectra of $Na_2YMg_2V_3O_{12}$ samples with their Gaussian components. (b) PLE and PL spectra of $Na_2YMg_2V_3O_{12}$:0.2Eu^{3+} phosphor. (c) PL spectra of $Na_2YMg_2V_3O_{12}$:xEu^{3+} phosphors at 365 nm for various doping concentrations. (d) Dependence of PL intensity on Eu^{3+} doping concentration.

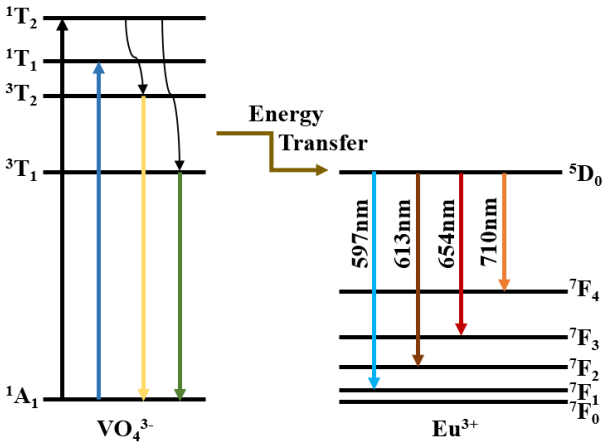

Fig. 3. Excitation and emission mechanisms of VO_4^{3-} and Eu^{3+}; energy transfer process among the corresponding energy levels.

To obtain further insight into the synthesised compounds, the PL decay curves of $Na_2YMg_2V_3O_{12}$:xEu^{3+} (x = 0, 0.04, 0.12, 0.20 and 0.24) phosphors were recorded at 530 and 613 nm under excitation at 365 nm. As revealed in Fig. 4(a), all normalised decay curves can be well fitted using the second-order exponential equation expressed in Eq. (2), and average decay times τ can be determined using Eq. (3)[33].

$$I_t = I_0 + A_1 \exp\left(-\frac{t}{\tau_1}\right) + A_2 \exp\left(-\frac{t}{\tau_2}\right), \quad (2)$$

$$\boldsymbol{\tau}^* = (A_1{\tau_1}^2 + A_2{\tau_2}^2)/(A_1\tau_1 + A_2\tau_2), \quad (3)$$

where I_t and I_0 are the emission intensities at time t and initial time, A_1 and A_2 are two constants, τ_1 and τ_2 are the fastest and slowest decay constants and τ^* is the effective decay time. With increasing concentration of Eu^{3+}, the τ^* values of host emission monotonically decrease from 2.42 to 2.37, 2.20, 2.16 and 2.05 μs for x = 0, 0.04, 0.12, 0.20 and 0.24, respectively. These results show that the matrix has photoluminescent properties. When doped with Eu^{3+}, the host emission lifetime decreases, further indicating the existence of energy transfer from $(VO_4)^{3-}$ to Eu^{3+}.

The normalised decay curves of Eu^{3+} emission monitoring at 613 nm are shown in Fig. 4(b). All decay curves consist of fast and slow decay components. Indeed, on the basis of the observation of the emission spectra of the host and samples doped with Eu^{3+} ions, the fast component can be attributed to host emission decay. The slow component corresponds to the decay of the $^5D_0$ level of Eu^{3+}. It is found that the slow curve follows single-exponential decay[34], i.e.

$$I_t = A\exp(-t/\tau) + I_0, \quad (4)$$

where I_t and I_0 are the emission intensities at time t and initial time, A is a constant and τ is decay time. According to this function, the average lifetimes of $Na_2YMg_2V_3O_{12}$:xEu^{3+} phosphors are determined to be 1.13, 1.06, 1.02 and 0.99 ms for x = 0.04, 0.12, 0.20 and 0.24, respectively. The PL lifetimes of $Na_2YMg_2V_3O_{12}$:xEu^{3+} are similar possibly because of the energy transfer behaviour between the vanadate host and Eu^{3+} ions.

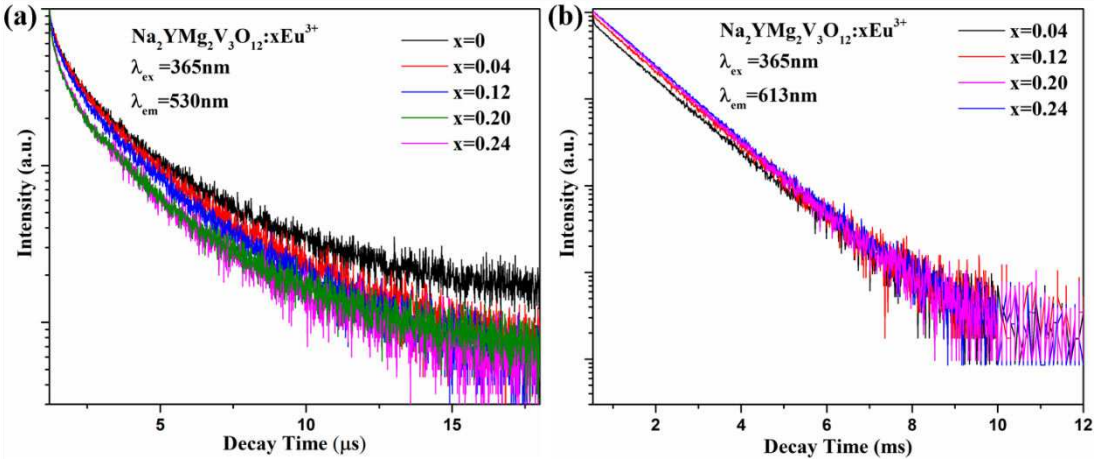

Fig. 4. Decay curves of $Na_2YMg_2V_3O_{12}$:xEu^{3+} for various Eu^{3+} concentrations x.

The colour coordinate for the $Na_2YMg_2V_3O_{12}$:$0.2Eu^{3+}$ phosphor is an important factor in the performance of phosphors, it was calculated, and it is shown in the CIE chromaticity diagram in Fig. 5. The colour coordinate for the $Na_2YMg_2V_3O_{12}$:$0.2Eu^{3+}$ phosphor under excitation at 365 nm was found to be (0.5843, 0.3683). This characteristic index indicates that the $Na_2YMg_2V_3O_{12}$:$0.2Eu^{3+}$ phosphor emits red light and that it can be used as a red-emitting

phosphor for WLEDs. The quantum yield is another important factor for phosphors applied in the field of WLEDs. The quantum yields of the $Na_2YMg_2V_3O_{12}:xEu^{3+}$ phosphors were recorded, and they are presented in the table inset in Fig. 5. Under excitation at 365 nm, the quantum yield values of $Na_2YMg_2V_3O_{12}:xEu^{3+}$ were found to be 11.9, 27.7, 45.4 and 52.4 for x = 0, 0.08, 0.12 and 0.20, respectively. These findings are also consistent with the variation in emission intensity across Eu^{3+} concentrations. These results reveal the potential applicability of this phosphor in near-UV chip excited WLEDs.

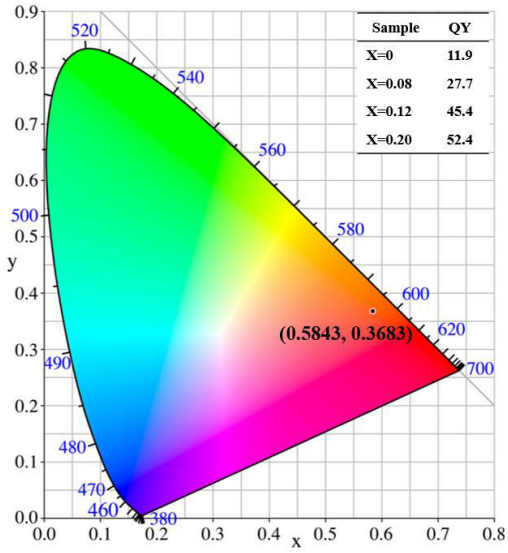

Fig. 5. CIE chromaticity coordinates for the $Na_2YMg_2V_3O_{12}:0.2Eu^{3+}$ phosphor. Inset table shows the quantum yield (QY) values for $Na_2YMg_2V_3O_{12}:xEu^{3+}$.

The high thermal resistance of phosphors is very important for the high optical performance of WLED devices and their consequent practical applicability in solid-state lighting[35]. The thermal quenching properties of the $Na_2YMg_2V_3O_{12}:0.2Eu^{3+}$ phosphor were tested by obtaining temperature-dependent emission spectra under excitation at 365 nm. As shown in Fig. 6, the emission intensity decreased smoothly with increasing temperature because of the increasing probability of non-radiative transition at high temperatures. The inset in Fig. 6(a) shows that the PL integral intensity at 100 °C retained approximately 73.59% of the initial intensity at room temperature. Notably, the emission positions changed little with increasing temperature in the temperature-dependent emission spectra. This favourable finding suggests colour stability for this phosphor across a range of operating temperatures.

To further investigate the temperature-dependent performance of this sample, the activation energy (ΔE) of the $Na_2YMg_2V_3O_{12}:0.2Eu^{3+}$ phosphor was calculated using the Arrhenius equation[36], i.e.

$$I(T) = \frac{I_0}{1+ce^{-\frac{\Delta E}{kT}}}, \quad (5)$$

where I_0 is the phosphor's maximum emission intensity at room temperature, I(T) is the intensity at a given temperature, c is a constant and k is the Boltzmann constant (8.629×10^{-5} eV). As shown in Fig. 6(b), the plot of $\ln[I_0/I(T) - 1]$ versus 1/kT is well fitted by a straight line. On the

basis of the slope of the fitted line, the ΔE value was determined to be 0.33 eV for excitation at 365 nm. This result indicates that the obtained $Na_2YMg_2V_3O_{12}:Eu^{3+}$ phosphors are of relatively good thermal stability, with great potential for use in WLEDs.

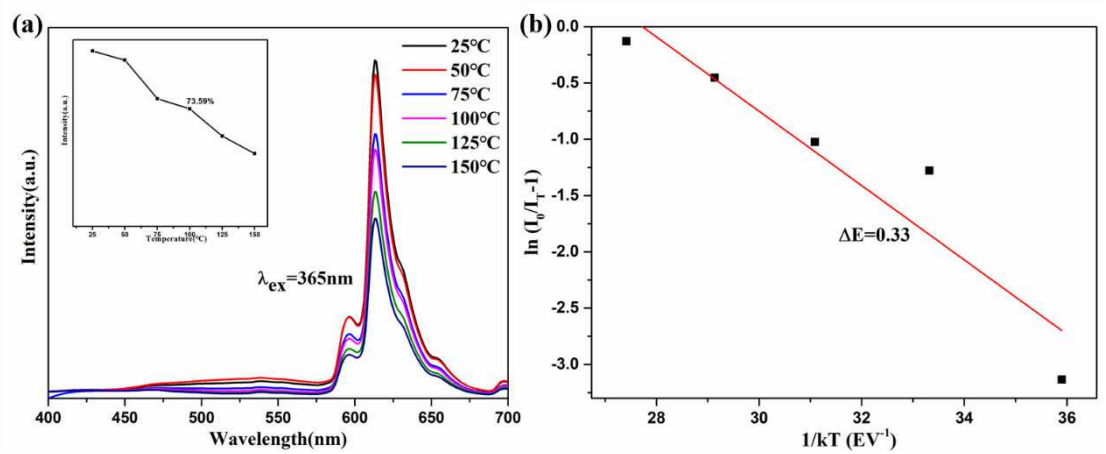

Fig. 6. (a) PL spectra (λ_{ex} = 365 nm) of the $Na_2YMg_2V_3O_{12}:0.2Eu^{3+}$ phosphor at various temperatures in the range of 25 °C–150 °C. Inset images in (a) show changes in PL intensity of $Na_2YMg_2V_3O_{12}:0.2Eu^{3+}$ with increasing temperature. (b) Dependence of $\ln[I_0/I(T) - 1]$ on 1/kT for the $Na_2YMg_2V_3O_{12}:0.2Eu^{3+}$ phosphor at the 613 nm emission peak.

To further demonstrate the feasibility of the as-prepared phosphors for solid-state illumination, a WLED device was designed and packaged based on an n-UV chip (365 nm) and an $Na_2YMg_2V_3O_{12}:0.2Eu^{3+}$ phosphor. To balance the colour combination and improve the Ra value of the LED, small quantities of commercial $(Ba,Sr)_2SiO_4:Eu^{2+}$ green phosphors and $BaMgAl_{10}O_{17}:Eu^{2+}$ blue phosphors were added, and a warm-white-emitting LED was fabricated. The electroluminescence spectra and photographs of the as-fabricated LED device are presented in Fig. 7, clarifying that the LED device's emitted light changed from red to white with the addition of green and blue phosphors. The CIE coordinates, Ra and CCT values of the white light generated from the LED device were (0.3068, 0.3491), 88.20 and 4460.52 K, respectively. These results demonstrated that the as-prepared phosphors are promising red-emitting phosphors for indoor solid-state illumination.

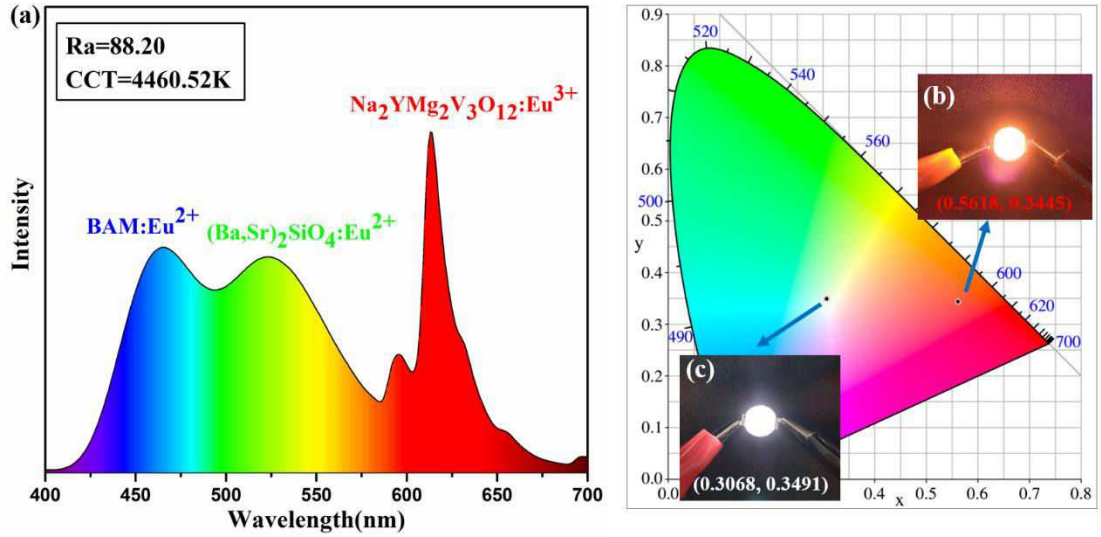

Fig. 7. (a) Electroluminescence spectra of a WLED combining 365 nm InGaN LED chips, as-prepared red $Na_2YMg_2V_3O_{12}$:0.2Eu^{3+} phosphor, a commercial blue $BaMgAl_{10}O_{17}:Eu^{2+}$ phosphor and a green $(Ba,Sr)_2SiO_4:Eu^{2+}$ phosphor with injunction current. (b) Chromaticity coordinates of red LED fabricated with $Na_2YMg_2V_3O_{12}$:0.2Eu^{3+} phosphor. (c) Chromaticity coordinates of the fabricated WLED.

4. Conclusions

A series of $Na_2YMg_2V_3O_{12}:Eu^{3+}$ vanadate phosphors were synthesised via solid-state reactions at 800 °C for 6 h. XRD results indicated that the as-prepared phosphors were crystallised in a single garnet structure with a cubic Ia3d (230) space group. Under excitation light in the UV region, self-activated emission of the $Na_2YMg_2V_3O_{12}$ host occurred at 530 nm. The broad emission band, ranging from 400 to 700 nm, is ascribed to the CT in the $(VO_4)^{3-}$ groups. The $Na_2YMg_2V_3O_{12}:Eu^{3+}$ phosphors showed both the broadband luminescence of the $(VO_4)^{3-}$ groups and the sharp peak emissions of Eu^{3+} ions, producing intense red light emission. Energy transfer occurred between the ^3T excited state of $(VO_4)^{3-}$ and the $^5D_0$ excited state of Eu^{3+}. The phosphors could also be excited by 365 nm light, and the optimum concentration of Eu^{3+} ions was around x = 0.20. Temperature-dependent emission spectra indicated good thermal stability for $Na_2YMg_2V_3O_{12}:Eu^{3+}$ phosphors. Finally, a WLED device based on an n-UV chip, the as-prepared $Na_2YMg_2V_3O_{12}$:0.2Eu^{3+} phosphor and $(Ba,Sr)_2SiO_4:Eu^{2+}$ and $BaMgAl_{10}O_{17}:Eu^{2+}$ phosphors produced an intense white light with CIE coordinates, Ra and CCT values of (0.3068, 0.3491), 88.20 and 4460.52 K, respectively. These results suggest the potential of $Na_2YMg_2V_3O_{12}:Eu^{3+}$ phosphor as a red-emitting phosphor for WLEDs and indoor solid-state illumination.

Acknowledgments

Supported by Qilu University of Technology (Shandong Academy of Sciences) integration of science, education and industry innovation pilot project (Grant No. 2020KJC-ZD12) and International Scientific and Technical Cooperation Project of Shandong Academy of Sciences (Grant No. 2019GHZD06).

Conflicts of interest

There are no conflicts to declare.

Reference

[1] Xia ZG, Liu QL. Progress in discovery and structural design of color conversion phosphors for LEDs. Prog Mater Sci 2016, **84**: 59-117.

[2] Ji HP, Zhang ZT, Xu J, et al. Advance in Red-emitting Mn^{4+}-activated Oxyfluoride Phosphors. J Inorg Mater 2020, **35**: 847-856.

[3] Ling JR, Zhou YF, Xu WT, et al. Red-emitting YAG: Ce, Mn transparent ceramics for warm WLEDs application. J Adv Ceram 2020, **9**: 45-54.

[4] He C, Ji HP, Huang ZH, et al. Preparation, structure, luminescence properties of europium doped zinc spinel structure green-emitting phosphor $ZnAl_2O_4:Eu^{2+}$. J Rare Earth 2018, **36**: 931-938.

[5] Liu X, Qian XL, Zheng P, et al. Composition and structure design of three-layered composite phosphors for high color rendering chip-on-board light-emitting diode devices. J Adv Ceram 2021, **10**: 729-740.

[6] Luchechko, A., Shpotyuk, Y., Kravets, O. et al. Microstructure and luminescent properties of Eu^{3+}-activated $MgGa_2O_4:Mn^{2+}$ ceramic phosphors. J Adv Ceram 2020, 9: 432–443.

[7] Dang PP, Liang SS, Li GG, et al. Full Color Luminescence Tuning in Bi^{3+}/Eu^{3+}-Doped $LiCa_3MgV_3O_{12}$ Garnet Phosphors Based on Local Lattice Distortion and Multiple Energy Transfers. Inorg Chem. 2018, **57**: 9251-9259.

[8] Han B, Dai YZ, Zhang J, et al. Luminescence properties of a novel yellow-emitting phosphor $NaLaMgWO_6:Dy^{3+}$. Mater Lett 2017, **204**: 145-148.

[9] Min X, Fang MH, Huang ZH, et al. Luminescent properties of white-light-emitting phosphor $LaMgAl_{11}O_{19}:Dy^{3+}$. Mater Lett 2014, **125**: 140-2.

[10] Min X, Sun YK, Kong LT, et al. Novel pyrochlore-type $La_2Zr_2O_7$: Eu^{3+} red phosphors: Synthesis, structural, luminescence properties and theoretical calculation. Dyes Pigments 2018, **157**: 47-54.

[11] Liu HK, Luo Y, Mao ZY, et al. A novel single-composition trichromatic white-emitting $Sr_{3.5}Y_{6.5}O_2(PO_4)_{1.5}(SiO_4)_{4.5}:Ce^{3+}/Tb^{3+}/Mn^{2+}$ phosphor: synthesis, luminescent properties and applications for white LEDs. J Mater Chem C 2014, **2**: 1619-1627.

[12] Wang ZW, Ji HP, Xu J, et al. Microsized Red Luminescent $MgAl_2O_4:Mn^{4+}$ Single-Crystal Phosphor Grown in Molten Salt for White LEDs. Inorg Chem 2020, **59**: 18374-18383.

[13] Min X, Fang MH, Huang ZH, et al. Synthesis and optical properties of Pr^{3+}-doped $LaMgAl_{11}O_{19}$–A novel blue converting yellow phosphor for white light emitting diodes. Ceram Int 2015, **41**: 4238-4242.

[14] Duke JDA, Muhammad GS, Sivakumar V. Synthesis and photoluminescence properties of Sm^{3+} substituted glaserite-type orthovanadates $K_3Y[VO_4]_2$ with monoclinic structure. J Lumin 2016, **177**: 104-10.

[15] Zhou ZP, Yu YS, Liu XT, et al. Luminescence enhancement of $CaMoO_4:Eu^{3+}$ phosphor by charge compensation using microwave sintering method. J Adv Ceram 2015, **4**: 318-25.

[16] Zhao M., Cao K., Liu MJ, et al. Dual-Shelled $RbLi(Li_3SiO_4)_2:Eu^{2+}@Al_2O_3@ODTMS$ Phosphor as a Stable Green Emitter for High-Power LED Backlights. Angew Chem Int Edit 2020, **59**: 12938-12943.

[17] Huang XY, Guo H. $LiCa_3MgV_3O_{12}:Sm^{3+}$: A new high-efficiency white-emitting phosphor. Ceram Int 2018, **44**:10340-10344.

[18] Jacob LA, Sisira S, Thomas K, et al. A reddish-orange emitting samarium doped α-$Na_3Y(VO_4)_2$ nanocrystals for single phased UV excitable white light applications. J Solid State Chem 2019, **280**: 120998.
[19] Zhou JC, Huang F, Xu J, et al. Luminescence study of a self-activated and rare earth activated $Sr_3La(VO_4)_3$phosphor potentially applicable in W-LEDs. J Mater Chem C 2015, **3**: 3023-3028.
[20] Chen W., Zhang J. Using nanoparticles to enable simultaneous radiation and photodynamic therapies for cancer treatment. J Nanosci Nanotechnol 2006, 6: 1159-1166.
[21] Liu YF, Chen W, Wang SP, et al. Investigation of water-soluble x-ray luminescence nanoparticles for photodynamic activation. Appl Phys Lett 2008, 92: 043901
[22] Phogat P, Khatkar SP, Malik RK, et al. Crystallographic and Judd-Ofelt Parametric investigation into $Ca_9Bi(VO_4)_7$:Eu^{3+} nanophosphor for NUV-WLEDs. J Lumin 2021, **234**: 117984.
[23] Zhou XJ, Zhang J, Chen LN, et al. $Sr_3Lu(VO_4)_3$: Eu^{3+} red-emitting phosphors for warm white LEDs. J Am Ceram Soc 2021, **104**:2721-2729.
[24] Zou XJ, Yao MZ, Ma L, et al. X-ray-induced nanoparticle-based photodynamic therapy of cancer. Nanomedicine 2014, **9**: 2339–2351
[25] Song D, Guo CF, Li T. Luminescence of the self-activated vanadate phosphors $Na_2LnMg_2V_3O_{12}$ (Ln=Y, Gd). Ceram Int 2015, **41**: 6518-6524.
[26] Zhao J, Guo CF, Li T, et al. Synthesis, electronic structure and photoluminescence properties of $Ba_2BiV_3O_{11}$: Eu^{3+} red phosphor. Dyes Pigments 2016, **132**:159-166.
[27] Pasinski D, Sokolnicki J. Nitridated $Ca_2NaMg_2V_3O_{12}$: Eu^{3+} Vanadate Garnet Phosphor-in-Glass. *Materials* 2020, ***13***: 2996.
[28] Hussain SK, Giang TTH, Yu JS. UV excitation band induced novel $Na_3Gd(VO_4)_2$:RE^{3+} (RE^{3+}= Eu^{3+} or Dy^{3+} or Sm^{3+}) double vanadate phosphors for solid-state lightning applications. J Alloy Compd 2018, **739**: 218-226.
[29] Rojas-Hernandez RE, Barradas NP, Alves E., et al. Up-conversion emission of aluminosilicate and titania films doped with Er^{3+}/Yb^{3+} by ion implantation and sol-gel solution doping. Surf Coat Tech 2018, **355**: 162-168.
[30] Tong Y, Chen YH, Chen SYZ, et al. Luminescent properties of $Na_2GdMg_2(VO_4)_3$:Eu^{3+} red phosphors for NUV excited pc-WLEDs. Ceram Int 2021, **47**:12320-12326.
[31] Zhou JC, Yao Y, Chen Y, et al. Synthesis, energy transfer mechanism, and tunable emissions of novel $Na_3La(VO_4)_2$:Re^{3+} (Re^{3+}= Dy^{3+}, Eu^{3+}, and Sm^{3+}) vanadate phosphors for near-UV-excited white LEDs. Ceram Int 2020, **46**: 6276-6283.
[32] Venkatesh BN, Jeyakumaran T, Ramaswamy S, et al. Synthesis and characterization of a Eu^{3+} -activated $Ba_{2-x}V_2O_7$: xEu^{3+} phosphor using a hydrothermal method: a potential material for near-UV-WLED applications. Luminescence 2021, **36**: 849-859.
[33] Min X, Fang MH, Huang ZH, et al. Luminescence Properties and Energy-Transfer Behavior of a Novel and Color-Tunable $LaMgAl_{11}O_{19}$:Tm^{3+}, Dy^{3+} Phosphor for White Light-Emitting Diodes. J Am Ceram Soc 2015, **98**: 788-794.
[34] Wang BC, Mi RY, Liu YG, et al. Identification of dual luminescence centers from a single site in a novel blue-pumped $Ca_3Sc_2Ge_3O_{12}$:Ce^{3+} phosphor. Dalton T 2019, **48**: 11791-11802.
[35] Zhao TX, Chen N, Du GP, et al. Effect of Ba^{2+} doping on the photoluminescence of YVO_4: Eu^{3+} phosphor and first principles calculations. J Lumin 2020, **222**: 117117.
[36] Liang YJ, Noh HM, Ran WG, et al. The design and synthesis of new double perovskite (Na,Li)YMg(W,Mo)O_6 :Eu^{3+} red phosphors for white light-emitting diodes. J Alloy Compd 2017,

716: 56-64.